Toward genome editing in X-linked RP—development of a mouse model with specific treatment relevant features

J. SCHLEGEL[1], J. HOFFMANN, D. RÖLL[2], B. MÜLLER, S. GÜNTHER, W. ZHANG, A. JANISE, C. VÖSSING, B FÜHLER, J. NEIDHARDT, H. KHANNA, B. LORENZ, and K. STIEGER

GIESSEN, BAD NAUHEIM, AND OLDENBURG, GERMANY AND WORCESTER, MASSACHUSETTS

Genome editing represents a powerful tool to treat inherited disorders. Highly specific endonucleases induce a DNA double strand break near the mutant site, which is subsequently repaired by cellular DNA repair mechanisms that involve the presence of a wild type template DNA. In vivo applications of this strategy are still rare, in part due to the absence of appropriate animal models carrying human disease mutations and knowledge of the efficient targeting of endonucleases. Here we report the generation and characterization of a new mouse model for X-linked retinitis pigmentosa (XLRP) carrying a point mutation in the mutational hotspot exon ORF15 of the *RPGR* gene as well as a recognition site for the homing endonuclease I-SceI. Presence of the genomic modifications was verified at the RNA and protein levels. The mutant protein was observed at low levels. Optical coherence tomography studies revealed a slowly progressive retinal degeneration with photoreceptor loss starting at 9 months of age, paralleling the onset of functional deficits as seen in the electroretinogram. Early changes to the outer retinal bands can be used as biomarker during treatment applications. We further show for the first time efficient targeting using the I-SceI enzyme at the genomic locus in a proof of concept in photoreceptors following adeno-associated virus mediated gene transfer in vivo. Taken together, our studies not only provide a human-XLRP disease model but also act as a platform to design genome editing technology for retinal degenerative diseases using the currently available endonucleases. (Translational Research 2019; 203:57–72)

[1]Current address: Internal Medicine, Faculty of Medicine, Justus-Liebig-University Giessen, Giessen, Germany.

[2]Current address: Deputy Animal Wellfare Officer, Faculty of Medicine, University of Münster, Germany.

From the Department of Ophthalmology, Faculty of Medicine, Justus-Liebig-University Giessen, Giessen, Germany; Max-Planck-Institute for Heart and Lung Research, Bad Nauheim, Germany; Department of Ophthalmology, University of Massachusetts Medical School, Worcester, Massachusetts; Human Genetics, Faculty of Medicine and Health Sciences, University of Oldenburg, Oldenburg, Germany; Research Center Neurosensory Science, University Oldenburg, Oldenburg, Germany.

Submitted for Publication November 22, 2017; received submitted August 16, 2018; accepted for publication August 16, 2018.

Reprint requests: Stieger K., Department Ophthalmology, Justus-Liebig-University Giessen, 35392 Giessen, Germany. e-mail: Knut.Stieger@uniklinikum-giessen.de.

1931-5244/$ - see front matter

https://doi.org/10.1016/j.trsl.2018.08.006

At A Glance Commentary

Schlegel J, et al.

Background
Genome editing in the retina is currently at the height of debate with regard to clinical translation, yet important aspects of the in vivo application are still poorly understood, in part due to the lack of animal models with human-like mutations.

Translational Significance
Our mouse model contains a human-like mutation in the RPGR-ORF15 gene, in which mutations in human cause XLRP. Due to its degenerative phenotype and the presence of an I-SceI restriction site, this mouse model is well suited to study the efficacy of all classes of endonucleases and to characterize the efficacy of therapeutic applications in retinal neurons in vivo.

INTRODUCTION

Retinitis pigmentosa (RP) is a group of heterogeneous disorders affecting primarily rod photoreceptors accounting for about 3 million patients worldwide. Mutations in the gene encoding the retinitis pigmentosa GTPase regulator (RPGR) are a major cause of RP in humans.[1] They account for 15%−20% of sporadic RP cases and up to 80% of all X-linked RP cases.[2,3] Patients typically suffer from early night-blindness with reduction of the visual field and reduced visual acuity, indicating an implication of both rods and cones in the pathology.[4] Optical coherence tomography (OCT) analyses show rapid loss of outer retinal structures that progresses over time.[5]

The *RPGR* gene consists of 19 exons and encodes multiple alternatively spliced isoforms. Two major RPGR isoforms $RPGR^{const}$ (encoded by 19 exons) and $RPGR^{ORF15}$ (terminates within intron 15) have been reported, the latter being uniquely expressed in photoreceptors.[6] Physiologically, both RPGR protein variants are located in the connecting cilium (CC) of the vertebrate photoreceptor, where they take part in a protein complex associated with the intraflagellar transport machinery that facilitates ciliary protein trafficking.[7-9] In addition, the $RPGR^{const}$ protein is also important for the transport of cargo toward the cilium via prenylation of the C-terminus by PDE6delta.[10]

Most of the disease-causing mutations in humans are found in $RPGR^{ORF15}$. The terminal exon ORF15 (exon 15+ part of intron 15) of the $RPGR^{ORF15}$ isoform is a mutational hot spot, accounting for >60% of *RPGR* mutations.[6] This exon consists of extensive purine-rich repeats and encodes for glycine (G) and glutamic acid (E) residues. The majority of the exon ORF15 mutations result in a frameshift due to deletions or duplications.[3] Although the mechanism of action of these mutations is not completely understood, an effect on the isoelectric point[11] or alterations in the post-translational modifications[12,13] of $RPGR^{ORF15}$ have been proposed.

Recently, several groups have shown the therapeutic effect of delivering the full-length $RPGR^{ORF15}$ with either wild type exon ORF15[14,15] or as a codon optimized version via adeno-associated virus (AAV) vector mediated gene transfer.[16] While production of a recombinant protein has been shown to restore function in the dog model of the disease (X linked progressive retinal atrophy, XLPRA2)[15] and in a knock out (KO) mouse model,[14,16] potential drawbacks with this form of treatment are always related to the artificial control of transgene expression or the interaction of residual endogenous protein with the recombinant protein.

In vivo genome editing represents a powerful tool to circumvent this issue, as it enables the correction of the disease-causing mutation in the genome, which would result in restoration of endogenous protein production. It is based on the cell's capacity to repair DNA double strand breaks (DSBs) by either error-prone nonhomologous end-joining (NHEJ), or in the presence of a template DNA by homology-directed repair or microhomology-mediated end-joining.[17] Induction of DSB at the target locus can be performed by specific endonucleases, of which a comprehensive toolbox exists, that is, homing endoncleases (HE) such as I-SceI, zinc-finger nucleases, TALE nucleases, or the CRISPR-Cas system.[18] However, size limitations in AAV vectors generate problems when TALE nucleases or CRISPR-Cas systems[19] are used together with the appropriate template DNA. Since HEs have been long considered to be un-programmable, they were not used to develop therapeutic strategies, even though their relatively small size and low toxicity render them an interesting tool. Recent progress in programming HEs for eukaryotic target loci may overcome this issue.[20]

Because the cellular DSB repair mechanisms are difficult to control in vivo and off target toxicity remains a major issue, current strategies to target exonic mutations in inherited retinal dystrophy genes in vivo are still comparably risky.[18] The absence of appropriate in vivo model systems to study genome editing in the retina in detail further complicates that issue. Standard knock-out models with large deletions or insertions in the genome do not represent ideal systems to study precise genome editing. Disease models based on point mutations are rare and only available for few inherited retinal dystrophies.[21]

Since most of the disease causing mutations in X-linked retinitis pigmentosa (XLRP) are located in the

RPGR-ORF15 exon and genome editing application are dependent on realistic animal model systems, the aim of this study was to develop a mouse model for XLRP containing a human-like mutation in the ORF15 exon that also contains specific features important for the development of therapeutic genome editing strategies. These features include a point mutation (deletion) similar to that in patients, other silent mutations for screening purposes and the introduction of an I-SceI recognition site in order to study this enzymes cutting efficiency in a therapeutically relevant system. Here we report the generation and characterization of a new mouse model of XLRP carrying a point mutation in exon ORF15 of the *Rpgr* gene and an I-SceI site downstream of exon ORF15, and provide evidence for NHEJ at the RPGR locus following I-SceI expression in cell culture and in photoreceptors in vivo following AAV mediated gene transfer.

MATERIALS AND METHODS

Ethics statement. The animals were maintained and experimental procedures complied in accordance with the Animal Welfare guidelines of the local German authorities and the ARVO Statement for the Use of Animals in Ophthalmic and Vision Research. The Institutional Animal Care and Use Committee of the local government approved all procedures (permission 22/2011 and 79/2016). Surgery and in vivo examinations were performed under anaesthesia and all efforts were taken to avoid suffering of the animals. Mice were euthanized by cervical dislocation. Mice were kept and bred in a 12-hour light and/or dark cycle with unlimited access to food and water in the animal facility of the Max-Planck-Institute for Heart and Lung Research in Bad Nauheim or in the animal facility of the Institute of Biochemistry at the Justus-Liebig-University Giessen.

Generation of the B6J.Sv129-Rpgr^{tm1Sti} mouse model. The generation of the targeting vector was done using the method of homologous recombination by gap repair.[22] A *bacterial artificial chromosome* BAC plasmid (pBACe3.6) containing the genomic locus of *Rpgr* was purchased from ImaGene GmbH (Berlin, Germany). A part of the genomic RPGR locus containing exons 13, *Orf14/15*, as well as a loxP/FRT flanked Neomycin cassette for positive selection were recombined via gap repair into the pKOIIV2 plasmid (kindly provided by Thomas Braun, MPI Bad Nauheim, Germany), already containing a DTA (diphtheria toxin A) cassette (Fig 1, A). To introduce the 4 mutations, the *Orf15* sequence was cloned into a pL452 plasmid[22] and the defined point mutations were integrated via mutagenesis polymerase chain reaction (PCR). The mutated target-sequence was cloned into the pKOIIV2 by directed cloning via Sal-I and Sac-II restriction digestion, thus finalizing the targeting vector.

For homologous recombination in embryonic stem (ES) cells, the targeting vector was linearized by NotI and electroporated into male ES cells (C57BL/6/129sv hybrid cells). Transgenic clones were selected by G418 resistance and screened for correct homologous recombination by long range PCR using primers binding within the Neomycin sequence [TTCTGAGGGGATCAATTCTCTAGAGCTCGC] and outside the recombination site [AGATCTGACGCCCTCTTCTGGTGTTTCTGAAG] (Fig 1, A, external sonde eS), and by standard PCR spanning 500 bp around the newly introduced XbaI site and the pathologic frame shift mutation (Fig 1, A, internal sonde iS) using primers [GGAAATGTAGTAGTGGAGCA] and [TTGATCCTCTGATGTGCCTT]. Presence of the I-SceI site was verified by PCR using primers [GATAATGAAAGTCAGGAAG] and [GGGTTATTGAATATGATCGGAATTGG] (Fig 1, B). Positive clones were injected into C57BL/6J blastocysts and F1 hybrid offspring was tested for the presence of DNA changes by PCR as described above. Genomic DNA was isolated from tail to tip tissue with the DNeasy Tissue Kit (Qiagen, Hilden, Germany). The neomycin cassette was deleted from the genome via Cre-recombination of the F1 hybrids. Offspring was subsequently back-crossed into a C57BL/6J background.

mRNA isolation and RT-PCR. RNA was isolated from collected neuroretinae homogenized by freeze and thaw cycles using liquid nitrogen. RNA was isolated using the AllPrep RNA/Protein Kit (Qiagen, Hilden, Germany).

For cDNA synthesis, 80 ng of total retinal RNA was reverse-transcribed using the PrimeScript cDNA Synthesis Kit (Takara, Saint-Germain-en-Laye, France). PCR amplification was performed using the PrimeScript Polymerase (Takara, Saint-Germain-en-Laye, France). The same primer pairs as for the initial screening (internal sonde iS) were used. Since the primers were placed outside the repetitive region and the PCR products were comparably small, we were able to generate sequencing data from gelpurified PCR products (Seqlab, Göttingen, Germany).

Western blot. Neuroretinae (n = 3) from 3 months old wild type, mutant, and age matched Rpgr^{ko}[23] animals were harvested and lysed using the RIPA (radioimmunoprecipitation assay) buffer. Fifty micrograms of total protein extract was analyzed by SDS-PAGE and immunoblotting using the RPGR^{ORF15} antibody, which identifies an epitope in the C-terminal region of the ORF15 frame, as described.[8] The antibody was kindly provided by Anand Swaroop (NEI).

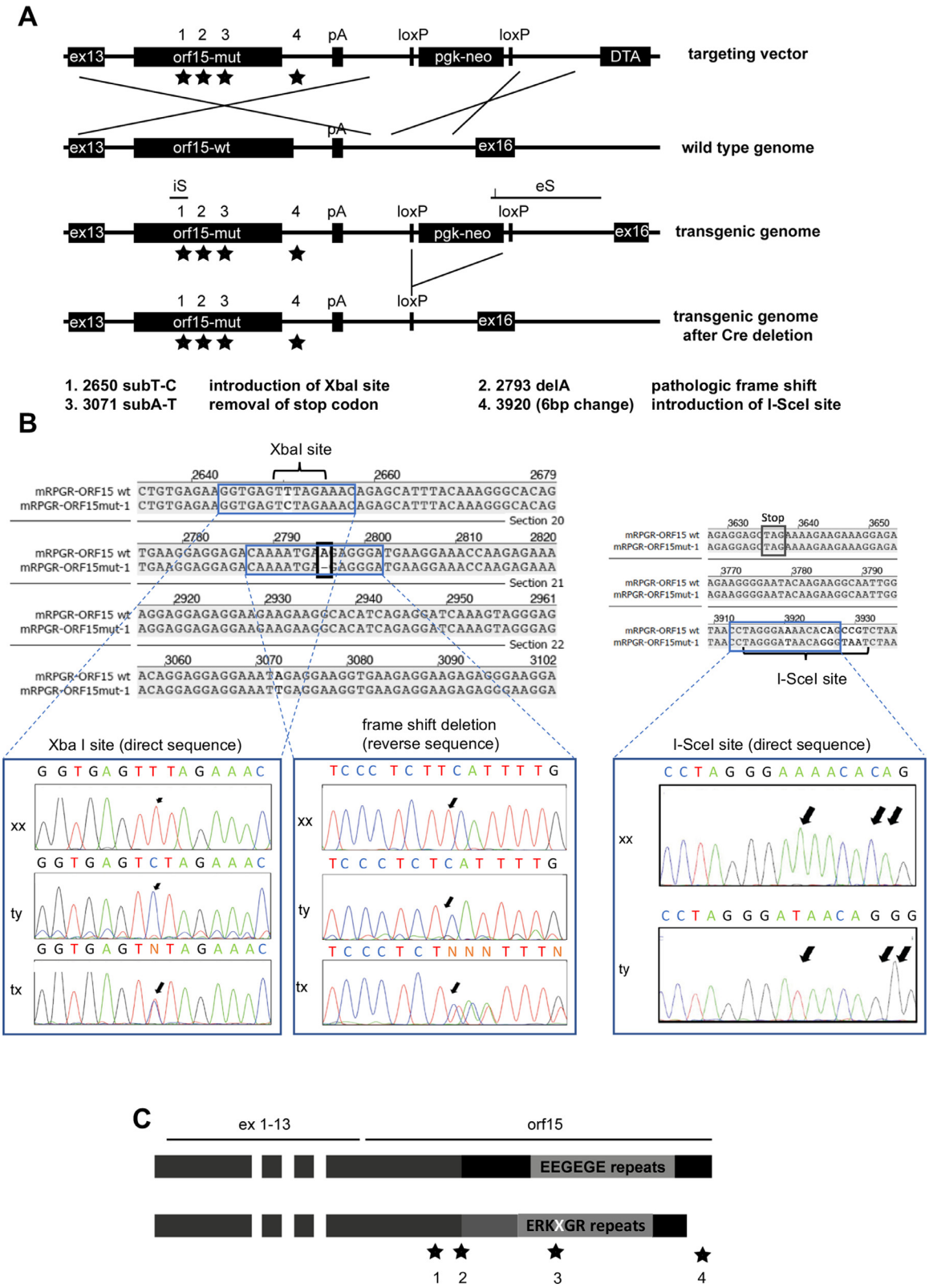

Fig 1. Generation of the mouse model. (**A**) Scheme of the recombination strategy of the targeting vector and the genomic mouse DNA applied for the generation of this mouse model. The locations of the mutational sites marked with asterisks and amplification sites for screening via PCR are indicated by brackets. The "floxed" neomycin-cassette is deleted via cre-recombination from the genome. Inserted mutations are specified by 1−4.

Immunofluorescence. Two different techniques were used to prepare the retinal tissue.

(1)
Enucleated eyes were embedded unfixed in OCT medium (optimal cutting temperature −20°C, Reichert Jung, Wetzlar, Germany) before preparing sections of 16 μm, which were subsequently fixed for 13 minutes at room temperature in 4% paraformaldehyde in 0.1 M phosphate buffered saline (PBS).

(2)
Eyecups were harvested and immediately fixed for 45−70 minutes in 4% paraformaldehyde. Eyecups were then cryo-protected in graded sucrose solutions. Vertical sections (16 μm) were cut with a cryomicrotome (SLEE Medical GmbH, Mainz, Germany) and collected on Superfrost slides.

Slides were incubated over night at 4°C with S1 and S3 rabbit polyclonal RPGR antibodies, diluted 1:200, or with a cocktail of rabbit polyclonal RPGR antibody and acetylated tubulin antibody, diluted 1:300 and 1:5.000 respectively. Primary antibodies were diluted in PBS containing 3% normal donkey serum (NDS) and 0.5% Triton X-100: S1 and S3 rabbit polyclonal RPGR antibodies were kindly provided by Dr. Tiansen Li (NEI). Rabbit polyclonal RPGR-ORF15 antibody targeting the C-terminal region of the ORF15 exon (see reference[8] for further information) was used as well. Monoclonal acetylated tubulin antibody was commercial (# T 6793, Sigma-Aldrich, Darmstadt, Germany). After washing with 0.1 M PBS, sections were incubated with Alexa-Fluor488 donkey antirabbit (1:500) secondary antibody (Molecular Probes, UK, Europe, #A21206) for 1.5 hours at room temperature. Nuclei were stained by DAPI (1 μg/ml; Molecular Probes, UK, Europe, #D1306) during incubation with secondary antibodies. For double immunolabeling, the respective primary and secondary antibodies were applied as a cocktail. Sections were mounted with antifade medium (Aqua Poly/mounting medium, Polysciences, #18606) and examined by laser scanning confocal microscopy (Olympus FV10i, Hamburg, Germany; equipped with argon and HeNe lasers).

Retinal histology. Enucleated eyes were fixed in yellow fix solution (45% formaldehyde, 45% PBS, 8% glutaraldehyde, and 2% picric acid) for 4 hours and rinsed in PBS overnight. The retinae were then post-fixed in 1% osmium tertoxide (2 hours) at pH 7.3, dehydrated in graded ethanols, and embedded in the EMbed-812 epoxy resin (all reagents from Science Services, Munich, Germany; automated LYNX-Tissue processor Leica, Bensheim, Germany). After 48 hours of heat polymerization at 60°C, semithin (0.5 μm) tissue sections were obtained and stained with toluidine blue. Pictures were taken with the Keyence BC8000 digital microscope (Keyence Inc, Japan).

Optical coherence tomography. The MICRON III fundus camera was used with modular spectral domain OCT technology (Phoenix Research Inc, CA), specifically developed for rodent applications (axial optical resolution 3 μm), and B scans were averaged over 10 frames. At least 3 animals per time point were analyzed over time. Total retina and outer nuclear layer (ONL) thickness were measured over the entire length of the scan (excluding the papilla in central scans) using the Insight OCT segmentation software (Phoenix Research Inc, Calif). Mean thickness and standard deviation was calculated from each group of animals. Significance was tested using a student t test with $P < 0.05$.

Electroretinography. Animals were anaesthetised by injection of xylazine (9 mg/kg body weight; 2% Xylazin, Ceva Santé Animale, Libourne, France) and ketamine (90 mg/kg body weight; 10% Ketavet # 9089.01.00, Bela-Pharm GmbH & Co. KG, Vechta, Germany). Full-field stimulation was performed using an Espion E^3 Electrophysiology system with a ColorDome full-field Desktop Ganzfeld stimulator (Diagnosys LLC, Lowell).

Mice were dark-adapted overnight and anesthetized under dim red light. Pupils were dilated with Tropicamide (1%, # 23.0311.03, Mydriaticum Stulln, Pharma Stulln, Stulln, Germany). For local anaesthesia Proparakain-Pos (0.5%, Ursapharm, Saarbrücken, Germany) was used in addition to Methocel (2%, # 421503, OmniVision GmbH, Puchheim, Germany) application to keep the cornea moist. A gold-wire ring electrode was used as recording electrode, and subcutaneous

below the scheme. The genomic modification was verified by sequencing an internal sonde (iS) and an external sonde (eS) (**B**) Confirmation of introduced sequence modifications by Sanger sequencing. An XbaI site was introduced as a silent substitution of a T by a C. The pathologic frame shift mutation was generated by deleting an A (represented by a missing T, because the sequencing was done on the reverse strand). The I-SceI site was introduced downstream of the reading frame in the mutant animal by exchanging 6 nucleotides. (**C**) Theoretical length and amino acid repeats in the RPGR-ORF15 protein. The EEGEGE repeats are changed to a ERKXGR repeat profile (where X stands for an K, R, or M amino acid), and the full length protein is supposed to be shorter compared to the wild type. DNA, deoxyribonucleic acid; PCR, polymerase chain reaction; RPGR, retinitis pigmentosa GTPase regulator; tx, heterozygous; ty, hemizygous mutant (mut); xx = homozygous wild type (wt).

needle electrodes as reference (between the ears) and ground (tail) electrode. Body temperature was maintained at 37°C using a heating pad.

Electroretinographies (ERGs) were performed as previously described.[24] Briefly, single flash recordings were obtained both under dark-adapted (scotopic) and light-adapted (photopic) conditions. Light adaption was performed with a background illumination of 30 cd/m^2 presented for 10 min. White stimuli were presented with increasing intensities, reaching from 10^{-4} cd s/m^2 to 25 cd s/m^2, divided into 10 steps of 0.5 and 1 log cd s/m^2. Twelve to fifteen responses were averaged with an interstimulus interval of 5 seconds or 17 seconds (for 1, 3, 10, and 25 cd s/m^2).

Significance was tested using a student *t* test with $P < 0.05$.

Targeting of the I-SceI site in vitro. The ORF15 exon from the targeting vector that was used to generate the mouse model was cloned into the pcDNA 3.1 (-) vector, under the control of a cytomegalovirus early enhancer promoter (CMV) promotor (Invitrogen/ThermoFisher SCIENTIFIC). Four micrograms of the vector was linearized with EcoRI and then transfected into HEK293 cells in a 6-well plate as mentioned earlier. Fourty-eight hours following the transfection, 0.5 μg/mL Geneticin (Life Technologies) was added to the medium for selection. Surviving cell foci were picked and transferred to 24 well plates. The selection process was repeated twice. The integration was analyzed using automated DNA sequencing by Sanger's methods.

I-SceI cDNA sequence was cloned into a bicistronic expression cassette together with the GFP cDNA separated by a T2A linker sequence under the control of a CMV promoter. After transfection of the expression plasmid into the HEK293$^{-mORF15}$ cell line, GFP positive cells were sorted 72 hours later by Fluorescent Activated Cell Sorting (FACS) and DSB repair events were analyzed using the T7 SURVEYOR assay (NHEJ events).

Targeting of the I-SceI site in vivo. The expression cassette CMV.I-SceI-T2A-GFP (the same as for the in vitro experiment) was cloned into an SSV9 vector. AAV2/5.CMV.I-SceI-T2A-GFP was produced in the Vector Core at the University Hospital of Nantes (http://www.vectors.nantes.inserm.fr) and the titer was determined by dot blot and expressed as vector genomes (vg)/mL. Viral preparation was manufactured using the HEK293 cell transfection method and purified by cesium chloride density gradients followed by extensive dialysis against PBS.

AAV2/8.RK.I-SceI-T2A-GFP was produced in the lab of John Neidhardt, Oldenburg. Here, the CMV promoter was replaced by the Rhodopsin kinase (RK) promoter within the SSV9 vector plasmid. Viral preparation was manufactured using the HEK293 cell transfection method and purified by ultracentrifugation on iodixanol gradient. Iodixanol gradient was exchanged by PBS and the titer was determined by quantitative PCR.

For transfer of AAV vectors into the subretinal space, 2-month-old mice (B6J.Sv129-Rpgr^{tm1Sti}) were anesthetized and pupils dilated as for the ERG measurements. A syringe (Hamilton, Reno, NV) with a blunt, GA34 12 mm needle (# 207434, Hamilton Company) was inserted tangentially through the conjunctiva and sclera and placed under visual control in the nasal half of the retina into the subretinal space (ie, between the retina and retinal pigment epithelium). One microliter vector suspension was injected to produce a bullous retinal detachment. Correct bleb formation was verified by OCT imaging immediately following the procedure.

Two months after injection, GFP expression was verified in vivo using the MICRON III camera (Phoenix Research lab). Animals were subsequently euthanized and the retina was dissociated. Dissociation was performed using the Papain-kit (Worthington Biochemical Corp) according to the protocol of the manufacturer with slight modifications. Briefly, retinae were kept for 90 minutes in Hanks balanced salt solution buffer at 37°C before being digested with Papain for 45 minutes at 37°C under constant shaking. DNAse digestion was performed in Earle's balanced salt solution together with Ocomucoid and bovine serum albumin, and cells resuspended after centrifugation in PBS.

Dissociated cells were sorted by FACS according to their GFP expression profile. Cells from the noninjected retinae were also FACS sorted according to their size and granulation (photoreceptor enrichment). DSB repair events were analyzed using the T7 SURVEYOR assay (NHEJ events).

RESULTS

Generation of the B6J.Sv129-Rpgr^{tm1Sti} mouse model. For the generation of the mouse model, a targeting vector containing a pathological point mutation (c.2793delA) was used for homologous recombination into the *Rpgr* locus of murine ES cells (C57BL/6/129sv hybrid cells)[22] (Fig 1, A, mutation 2). To obtain an extended altered amino acid chain caused by the frame-shift mutation, the conditioned formation of a premature stop codon was prevented by introduction of an additional single base substitution (c.3071subT-A) (Fig 1, A, mutations 3). Furthermore, an XbaI restriction site (silent mutation, no change of encoded amino acid) was introduced for later screening purposes (c.2650subT-C) (Fig 1, A, mutations 1). Since the newly generated mouse model was created to be used for the development of therapeutic strategies based on genome editing, a recognition site for the I-SceI homing-endonuclease was integrated into the genome downstream of the Orf15 stop codon in the mutant sequence (Fig 1, A, mutation 4).

Successfully recombined stem cells were implanted into surrogate BALB/c mother mice and offspring was screened for chimeric events and sequence changes on the X chromosome. F1 offspring carrying the targeted mutations on the X chromosome was crossed with Cre-deleter mice to remove the neomycine selection cassette and further breeding was performed into the C57BL/6J background. Sequence changes were verified at the genomic level through Sanger sequencing during the breeding process (Fig 1, B). The entire sequence of the putative mutant full length cDNA is provided in the Supplementary file 1.

The resulting mutant protein is considered to contain RK repeats instead of EG repeats and is slightly shorter compared to the wild type protein (Fig 1, C). The amino acid sequence of the putative full length RPGR^{ORF15} isoform is shown in Supplementary file 2.

Expression of the mutant allele and protein in the mouse model. Expression of the targeted *Rpgr*^{Orf15} allele was verified on RNA and protein level. Messenger RNA (mRNA) from neuroretinae of mutant and wild type animals was used as a template for cDNA synthesis via reverse transcription. A PCR product of 500bp in size was generated from the region containing the pathological mutation (2793delA) (Fig 2, A), and was sequenced to verify the alteration of the sequence (Fig 2, B).

Translation of mRNA into protein was verified on whole retina extracts from animals at the age of 3 months using an antibody that recognizes an epitope in the C-terminal part of the ORF15 exon, thus allowing to recognize the RPGR^{ORF15} isoform specifically (Fig 2, C). As a control, protein from age matched Rpgr^{ko} mouse retinae was used.[23] Bands with sizes below and above 150 kD were detected in the wild type retina, indicating the presence of several ORF15 variants with alternative amounts of the ORF15 acidic domain. In contrast, in the mutant retina, the total amount of RPGR protein was lower, and some of the isoforms appeared to be absent from the blot. The largest band, widely considered to be the RPGR-ORF15 full length band was visible in both samples, with the size in the mutant sample being slightly higher, potentially associated with the lower amount of acidic amino acids being present in this protein.

Expression and localization of the different RPGR isoforms was subsequently analyzed on retinal frozen sections of 3-month-old animals (Fig 3). First, we employed the same ORF15 specific antibody as was used in the Western blot together with an antibody staining acetylated tubulin, which marks the CC (Fig 3, A and B). The difference in immunolabeled RPGR-ORF15 protein between wild type and mutant retina was obvious. In the wild type retina, RPGR^{ORF15} immunoreactivity (green color) was of rod-like shape with brighter small spots (Fig 3, A, zoomed inserts). It was visible at the OS-axoneme side of almost every single Actub immunoreactive CC (red color). At the distal end of the immunolabeled CC, a small area of co-localization of RPGR^{ORF15} and Actub was visible (orange color). Similarly, albeit more spot-like, staining of RPGR^{ORF15} was detectable at the OS-axoneme side of the Actub immunoreactive CC in the mutant retina, the majority of it being correctly localized to the CC but with reduced immunoreactivity (zoomed inserts). In addition, exceptionally long rod-like accumulations of immuno-labeled RPGR^{ORF15} have been observed on the distal side of the CC, more frequently in the mutant than wild type retina. Since background signal was observed in both wild type and mutant outer retina, mislocalization of RPGR^{ORF15} was not assumed.

To further characterize the expression and localization of both isoforms, we also used S1 and S3 antibodies that have been widely used to stain RPGR proteins in the retina. The S1 antibody, which recognizes both the RPGR^{ORF15} as well as the RPGR^{const} variant, detected RPGR protein in both wild type and mutant animals at the IS-side of the CC co-localizing with the Actub antibody (Fig 3, C and D). The reduced RPGR$^{ORF15+const}$ immunoreactivity in mutant animals was due to the more spot-like appearance (Fig 3, D).

Staining with the antibody S3, which recognizes only the RPGR^{const} variant, revealed clear immunolabeling in the wild type and mutant retina co-localizing with the Actub antibody at the IS-side of the CC (Fig 3, E and F). In the mutant retina RPGR^{const} staining had a bright and rod-like appearance and was visible in every Actub immunoreactive CC. In comparison to the wild type retina, it appeared to be slightly more intense. The spot-like appearance of RPGR^{const} immunoreactivity in the wild type retina resulted in a less prominent fluorescence than RPGR$^{ORF15+const}$ immunolabeling (Fig 3, C).

In summary, these data demonstrate the expression and translation of mutant RPGR^{ORF15} mRNA. The RPGR^{const} isoform is unaltered in its location but seems to be potentially upregulated when detected by

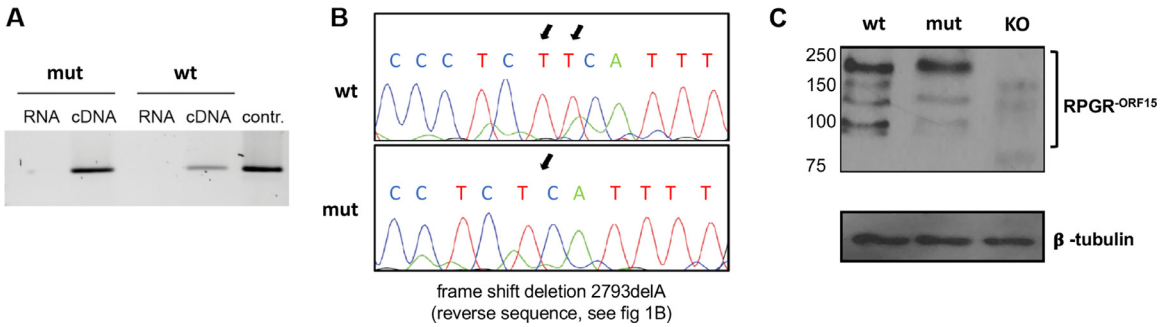

Fig 2. Verification of transgene expression in the retina. (**A**) For the verification of the expression of the transgene in the retina, mRNA samples from retinal extracts were transcribed via reverse transcription and subsequently amplified via PCR. As controls mRNA samples were used as PCR template to check them for contaminations of genomic DNA, which could lead to inaccurate test results. (**B**) PCR products were checked for the mutational sites using direct Sanger sequencing. The comparison of the histograms shows the pathological point mutation (an adenine deletion sequenced on the complementary strand and therefore displayed as thymine deletion.) (**C**) Western blot of retinal extracts (~100 μg) from wild type (wt) and mutant (ty), and as negative control from *Rpgr*^{ko} (KO) mice at the age of 3 months probed with the RPGR^{ORF15} specific antibody. Immunoblot of the same samples with anti-*β*-tubulin antibody served as loading control. DNA, deoxyribonucleic acid; PCR, polymerase chain reaction; RPGR, retinitis pigmentosa GTPase regulator.

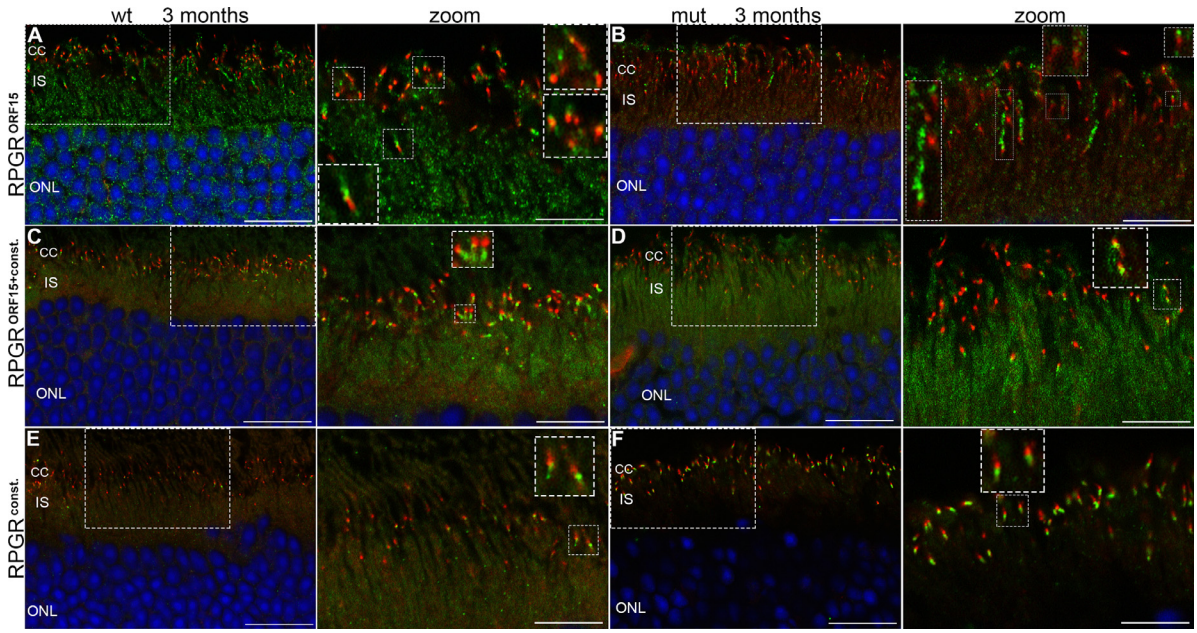

Fig 3. RPGR protein localization in the retina. (**A, B**) 16 μm sections of wild type (wt) and mutant (mut) animals at 3 months of age double immunostained with the RPGR^{ORF15} specific antibody recognizing the C-terminal part of the ORF15 region[8] and the monoclonal acetylated tubulin antibody (Actub), a marker for the CC. Nuclei were stained using DAPI (blue). Low levels of background staining is visible in the inner segment area. RPGR^{ORF15} (green) is visible at OS-axoneme side of the Actub immunoreactive CC (red). Inserts in A and B are zoomed in two-fold (zoom column). Individual immuno-labeled CC are zoomed in further (2-fold; insets within the zoom column). (**A**) A small area of co-localization of RPGR^{ORF15} and AcTub was visible at the OS-axoneme side of the Actub immunoreactive CC (orange color). (**B**) RPGR^{ORF15} immunoreactivity appears reduced and more spot-like but correctly localized to the CC. In addition, exceptionally long rod-like accumulations of immunolabeled RPGRORF15 can be observed on the OS-axoneme side of the CC, more frequently in the mut than wt retina. Some background signal was observed in both wt and mut outer retina with the RPGR^{ORF15} antibody. (**C**−**F**) 16μm sections of wild type and mutant animals at 3 months of age were stained with either S1 (**C, D**) or S3 (**E, F**) antibody, recognizing both the RPGR^{ORF15} and the RPGR^{const} isoform, or only RPGR^{const}, respectively. Inserts in all images show a two-fold magnified region with co-localization of the RPGR antibody with the Actub antibody (zoom column). Individual immuno-labeled CC are zoomed in further (two-fold; inserts within the zoom column). (**C**) In wt retina RPGR$^{ORF15+const}$ immunoreactivity (green) has a rod-like shape at the IS-axoneme side of the Actub immunoreactive CC (red). (**D**) In mut retina RPGR$^{ORF15+const}$ immunoreactivity appears more spot-like and therefore reduced. (**E**) In wt retina RPGR^{const} immunoreactivity shows spot-like appearance (**F**) In the mut retina RPGR^{const} staining has a bright and rod-like appearance and is visible in every Actub immunoreactive CC. Therefore, RPGR^{const} immunoreactivity appears to be up-regulated in comparison to the wt retina. Compared to the RPGR^{ORF15} antibody (**A,B**) the background signal of the RPGR$^{ORF15+const}$ and RPGR^{const} immunostaining is very little in both wt and mut ONL retina. In mut retina RPGR^{cons} showed almost no background labeling at all. CC: connecting cilium; IS: inner segments; ONL: outer nuclear layer; OS: outer segments; RPE: retinal pigmented epithelium; RPGR, retinitis pigmentosa GTPase regulator; Scale bars: 20 μm in A−F; 10 μm in all zoom columns. (Color version of figure is available online.)

the RPGR^{const} antibody. The 2 RPGR^{ORF15} antibodies applied in this study to detect the RPGRORF15 protein revealed different subciliary localizations in both the wild type and mutant retina. While this might be due to technical reasons with the postfixation technique, it can also be associated with different epitopes recognized in different RPGR^{ORF15} isoforms as seen in our immune blot results (Fig 2, C). Further studies are ongoing to shed more light on this observation.

Significant reduction of retinal layer thickness starting at 9 months. Initially, the retina was analyzed at young age (3−6 months) and old age (15−18 months) for changes to the gross retinal morphology (Fig 4, A−D). In young mutant retinae, the gross morphology was similar to healthy retinae, with the exception that the outer segments looked slightly disorganized (Fig 4, A and B). Older mutant retinae displayed significant structural changes compared to healthy retinae, including a loss of column like organization of the nuclei, and outer segment destruction (Fig 4, C and D). No morphologic changes in the inner nuclear layers (ganglion cell layer) were observed in mutant animals (data not shown). Quantification of photoreceptor cell nuclei showed a slight loss of nuclei at early ages (3−6 months) in mutant retinae, which increased over time and aggravates at late ages (18−21 months), where only about 50% of nuclei were left (Fig 4, E).

In order to monitor photoreceptor degeneration over the entire lifetime of the animals, we performed in vivo imaging of the retina using OCT (Fig 5). Retinae were examined starting at 3 months up to 24 months of age every 3 months in the center and midperiphery (5 disk diameter distance; Fig 5, A and B). From the earliest time point onwards (even at 1 month, data not shown), the outer retinal bands, which can be nicely seen in wild type retinae, were not

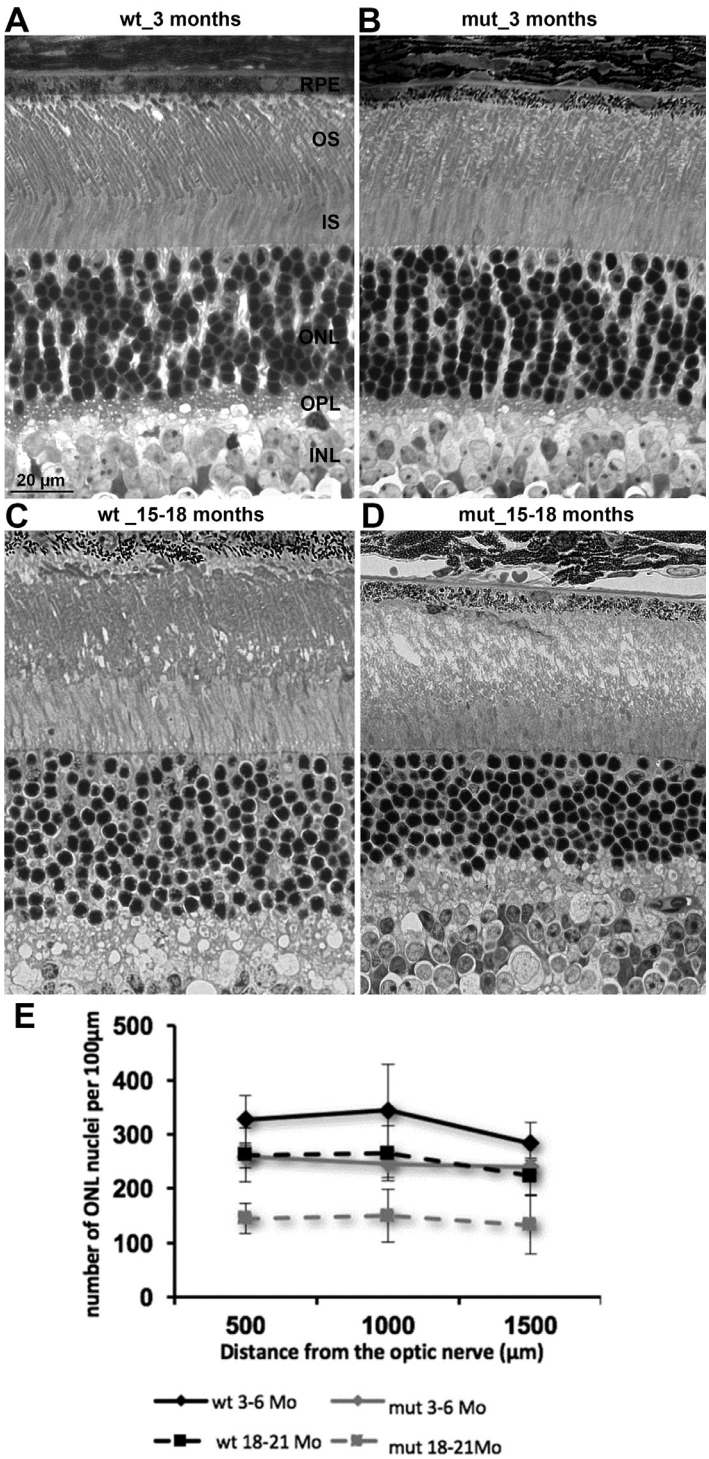

Fig 4. Analysis of the retinal morphology. Semithin sections reveal morphologic alterations in the retinae of mutant mice. (**A, B**) Retina of a wild type animal at 3 and 18 months of age. (**C, D**) Retina of mutant animals at 3 and 18 months of age. (**E**) For the quantification of photoreceptor nuclei the number of nuclei in a section of 100 µm was counted at defined distances from the optic nerve head (n = 2 animals per group). Standard deviations are shown. INL: inner nuclear layer; IS: inner segments; ONL: outer nuclear layer; OPL: outer plexiform layer; OS: outer segments; RPE: retinal pigmented epithelium.

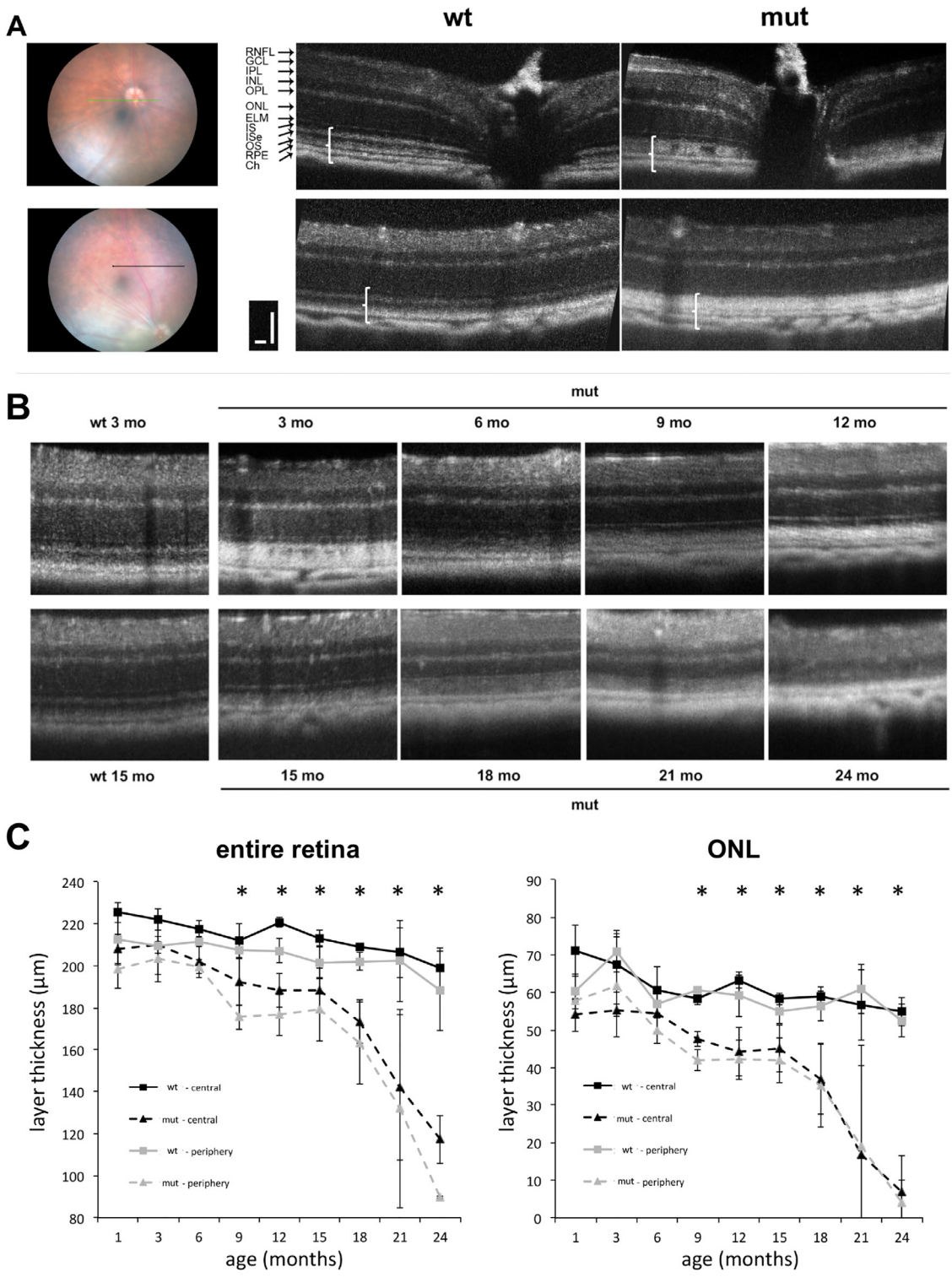

Fig 5. *In vivo* imaging of the retina using optical coherence tomography (OCT). (**A**) Retina of wild type and mutant animals were examined in the central or peripheral part (5 disk diameter distance) of the retina. The white brackets in the B scans indicate the outer retinal bands region. The green or black line in the fundus photographs highlights the area where the OCT scans was obtained. Scale bar: 50 µm. (**B**) Timeline of OCTs from the peripheral scans from wild type animals (3 and 15 months) and from mut at 3, 6, 9, 12, 15, 18, 21, and 24 months. (**C**) Entire retina and ONL thickness in wild type and mutant animals were quantified between 3 and 24 months of age (n = 4 animals per group). CH: choroid; ELM: external limiting membrane; GCL: ganglion cell layer; INL: inner nuclear layer; IPL: inner plexiforme layer; IS: inner segments; ISe: inner segments ellipsoid;

discernable in the mutant retina (Fig 5, A, white brackets in OCT scans). These findings confirm the observation of outer segment disorganization in mutant animals as seen in Fig 4, B and represent an early biomarker for morphologic changes in the retina.

The thickness measurements of the entire retina as well as ONL alone show a progressive thinning of the layers, which becomes significant at the age of 9 months (Fig 5, B and C). Both, entire retina and ONL thickness in the center as well as the periphery are initially slightly thinner in mutant retina with a first decline at 9 month followed by a plateau phase until 15 months. Beyond that age, entire retina and ONL thickness rapidly decline until only minimal ONL thickness is left at 24 months of age and the entire retina thickness is only 50% of normal.

Significant reduction of functional changes starting at 12 months. Retinal function was analyzed using standard ERG recordings at different ages between 1 and 21 months (Fig 6). In the dark-adapted ERG, responses show progressing decrease of the a-wave amplitude, starting to be significant at the age of 12 months (Fig 6, A, B, and H). At 21 months, only about 35% of normal a-wave amplitudes were reached in mutant animals. B-wave amplitudes also decrease progressively starting at 12 months of age (Fig 6, C). The b/a-wave ratio remained unchanged at about 2, indicating a progressive degeneration of photoreceptors and second order neurons over time (data not shown). Albeit the amplitudes were decreased, characteristic waveforms remained in a-waves as well as in b-waves including oscillatory potentials (Fig 6, A and B). Interestingly, a-wave latency was increased in older mutant animals compared to age matched control mice (data not shown).

Under photopic conditions, b-wave amplitude was also slightly, but not significantly decreased in mutant animals (Fig 6, D and E). Photopic flicker responses were severely reduced in older animals (18−21 months) but not in young animals (3−6 months) (Fig 6, F and G).

DNA repair at the I-SceI locus in vitro and in vivo. In order to perform a proof of principle experiment demonstrating the possibility to edit the genome at the I-SceI locus, we employed a HEK293 cell line containing the C-terminal part of the murine ORF15 exon (Fig 7, A). A vector cassette containing the I-SceI and GFP cDNA linked by a T2A peptide under the control of a CMV promoter was used (Fig 7, B). Upon transfection, we subsequently enriched the transfected cell population to be analyzed by cell sorting of GFP positive cells (FACS). Upon enrichment, the surveyor assay (T7E1) was performed to visualize NHEJ events, which were at relatively high levels in the enriched cell population (Fig 7, C). Since nonenriched samples lower levels of NHEJ events, this method to isolate endonuclease expressing cells is important to obtain larger number of DNA editing events.

Upon successful proof of concept in in vitro experiments, we further evaluated the possibility to use I-SceI mediated genome editing at the ORF15 locus in vivo. One microliter each of AAV vectors (titer = 3×10^{11} vg/mL) containing the I-SceI-T2A-GFP expression cassette either under the control of the ubiquitous CMV promoter (AAV2/5) or the photoreceptor specific RK promoter (AAV2/8) was subretinally administered into the $Rpgr^{tm1Sti}$ mouse retinae at 8 weeks of age (Fig 8, A). Two months later, GFP expression was verified by in vivo fluorescent imaging (Fig 8, B), and retinal cells were dissociated and FACS enriched for GFP expression (Fig 8, C). Noninjected eyes were sorted for size and granulation. The enriched cells were subjected to the surveyor assay (T7E1) showing evidence of NHEJ activity at the target locus only in the injected eyes. Control vectors containing exclusively the GFP cDNA under the control of a CMV promoter were also injected into control animals, and did not show any sign of NHEJ events in the surveyor assay (data not shown).

DISCUSSION

In this study, we describe a new mouse model for human XLRP, which contains a single pathologic point mutation in the Rpgr-Orf15, a genetic alteration found frequently in human patients. We observed expression and limited translation of the mutant Rpgr-Orf15 transcript, and a slowly progressive degeneration starting at the photoreceptor level at about 9 months of age, both morphologically and functionally. Furthermore, we show for the first time in vivo genome editing at the Rpgr-ORF15 locus by using the I-SceI endonuclease.

The uniqueness of the presented mouse model lies in the presence of an I-SceI site close to the Rpgr gene locus, which can be used in subsequent experiments to study the efficacy of genome editing approaches based on homing endonucleases (HE) or other systems. Since the I-SceI endonuclease has a longstanding history in showing high efficacy and low toxicity in eukaryotic cells, this nuclease can now be used as a reference standard for studies using the current state of the art RNA based endonuclease systems (ie, CRISPR-Cas). Recent developments in the research for HE point even toward programmable variants, making our model even more relevant for future studies. Furthermore, due to its small size, HE including I-SceI is the single nuclease class that can be packaged into one single AAV vector together with the template DNA, which allows us to study the importance of using a 1-vector system compared to a 2-vector system, a question that is currently unanswered due to the lack of useful models and nucleases. In vivo studies addressing this question are currently ongoing.

Even though the Rpgr-ORF15 sequence is optimal for genetic modifications due to its highly repetitive nature, replacement of the entire exon by homology-directed repair or microhomology-mediated end-joining could be envisaged as one treatment approach for a large number of patients with different mutations within that exon. Therefore, targeting this exon by HE or other systems in a relevant animal model is of high interest to the scientific community.

In our mouse model, we observed protein translation from the mutant $Rpgr^{Orf15}$ transcript. This is in slight contrast to the situation observed in the *rd9* mouse model, which contains a 32 bp deletion in the ORF15

ONL: outer nuclear layer; OPL: outer plexiforme layer; OS: outer segments; RPE: retinal pigmented epithelium; RNFL: retinal nerve fiber layer; * $P < 0.05$. (Color version of figure is available online.)

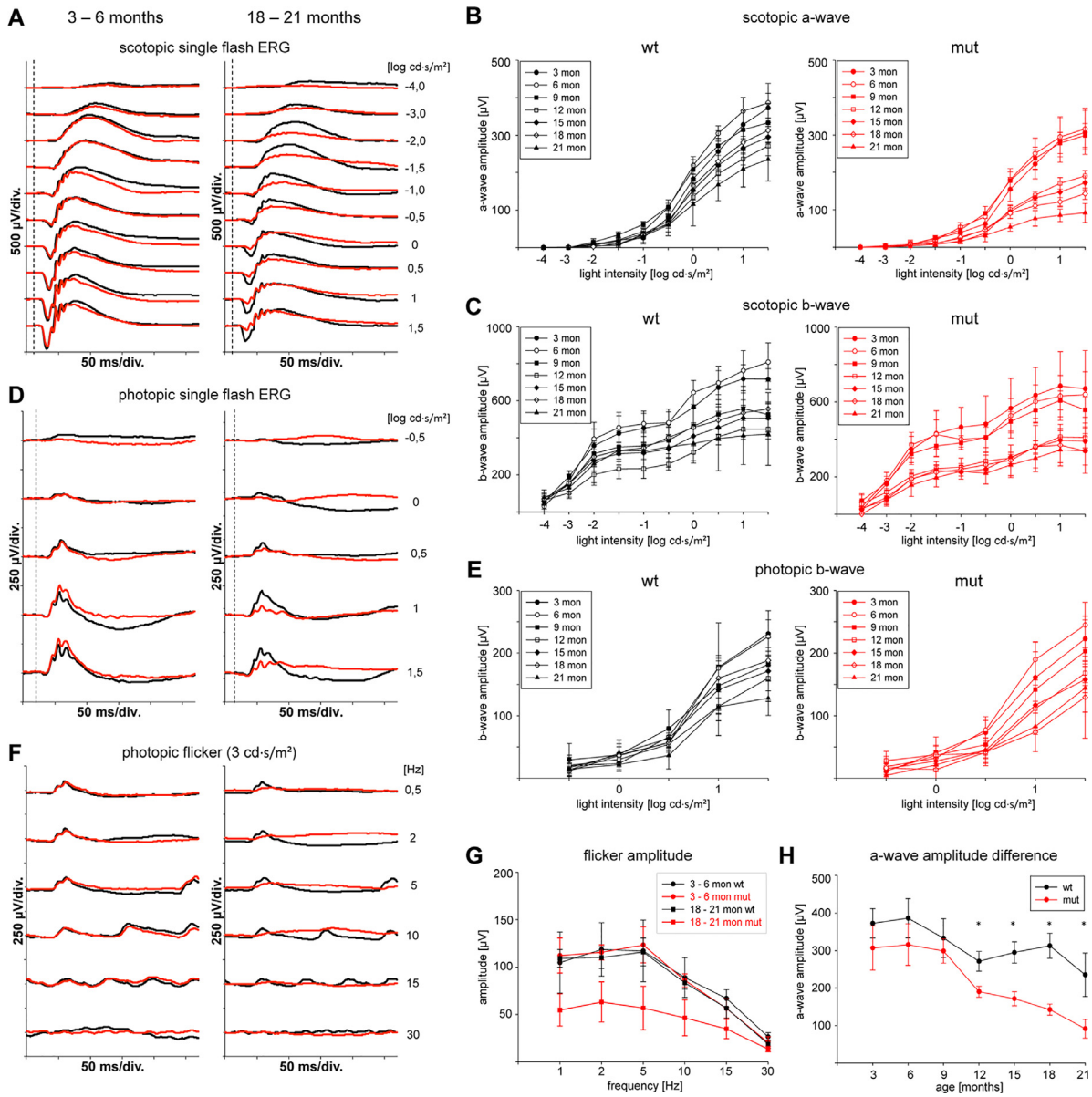

Fig 6. Functional examination using electroretinography (ERG). (**A**) Representative scotopic single flash recordings of young (3−6 months of age) and old (18−21 months of age) wild type (wt) and mutant (mut) animals. (**B**) Scotopic a-wave amplitudes separated for each flash intensity for wild type (wt) and mutant (mut) animals between 3 and 21 months of age (n =4 animals per time point). (**C**) Scotopic a-wave amplitudes separated for each flash intensity for wild type (wt) and mutant (mut) animals between 3 and 21 months of age (n = 4 animals per time point). (**D**) Representative photopic single flash recordings of young (3−6 months of age) and old (18−21 months of age) wild type (wt) and mutant (mut) animals. (**E**) Photopic a-wave amplitudes separated for each flash intensity for wild type (wt) and mutant (mut) animals between 3 and 21 months of age (n = 4 animals per time point). (**F**) Representative photopic flicker responses of young (3−6 months of age) and old (18−21 months of age) wild type (wt) and mutant (mut) animals. (**G**) Correlation of photopic flicker amplitude and flicker frequency in wild type and mutant animals at young (3−6 months) and old (18−21 months) age. (**H**) Correlation of scotopic a-wave amplitudes with age. Differences between wild type and mutant animals start to be significant at 12 months of age. * $P < 0.05$.

region leading to a frame shift similar to our model and which shows only residual levels of the mutant protein in western blot and immunofluorescence assays.[25] Furthermore, normal amounts of the RPGR^{const} isoform were produced and are correctly localized in the CC in our mouse model, while no S3 antibody staining was detected in the rd9 mouse.[25] A possible reason for this difference could be a differential regulation of the

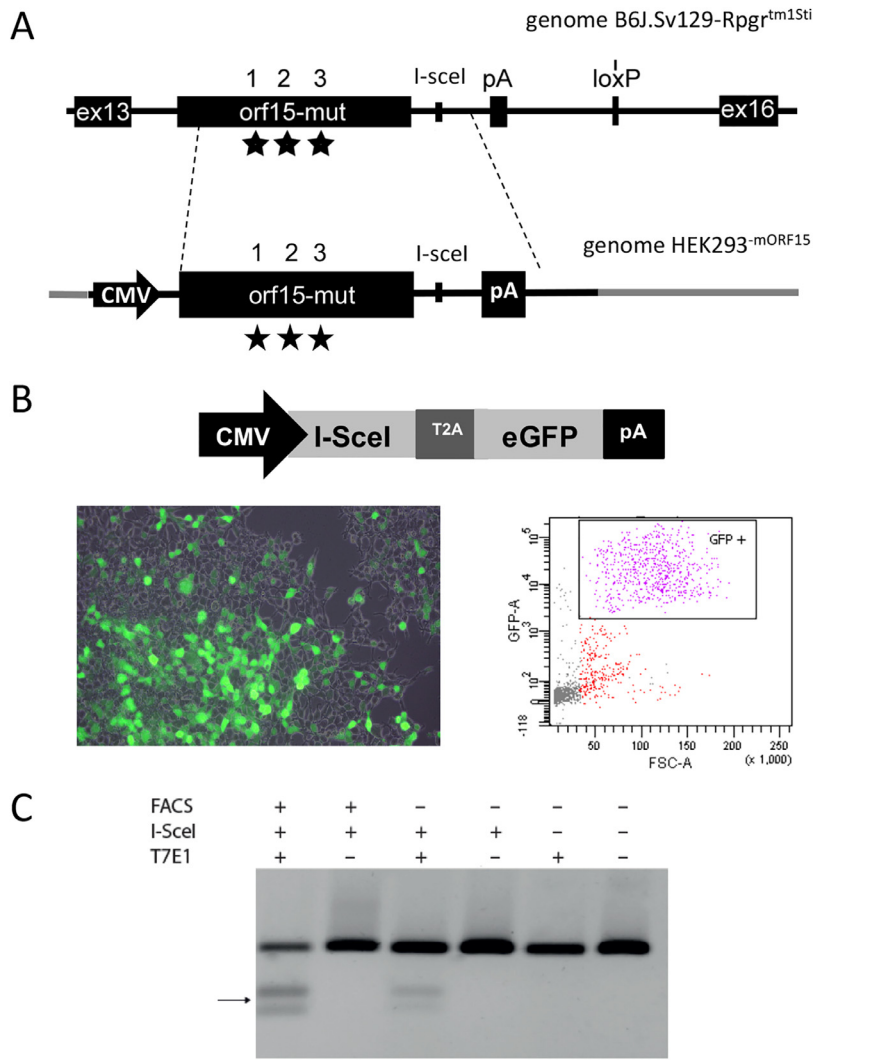

Fig 7. Genome editing at the I-SceI site in vitro. (**A**) Scheme of the generation of the cell line HEK293$^{-mORF15}$ by cloning the mutant RPGR-ORF15 region into the HEK293 cell line under the control of a CMV promoter. Stars indicate the point mutations integrated into the ORF15 sequence. (**B**) The vector plasmid contains the I-SceI cDNA linked with the GFP reporter gene by a T2A linker und the control of a CMV promoter, thus allowing production of equal amounts of protein. Microscopy image shows the green fluorescent cells after transfection. FACS data show the enrichment of the GFP positive cell population. (**C**) Visualization of the DNA repair events following transfection of the cell line with the plasmid vector and subsequent enrichment of the GFP positive cells. T7 surveyor assay demonstrates NHEJ activity at the target site in the GFP enriched cell population and to a lower extend in the transfected cells without GFP enrichment. "+" and "−" refers to whether FACS enrichment, I-sceI expression and T7 endonuclease digestion took place or not.

RPGR^{const} isoform in both disease models, a mechanism already seen in selective KO models of either Rpgr^{const} or Rpgr^{Orf15}.[26] Further studies to decipher this potential mechanism are currently ongoing.

We observed thinning of the ONL and reduction of photoreceptor nuclei at later stages of the disease. In the context of a therapeutic setting, such late reductions of photoreceptor cells and function may not be advantageous, since readout parameter following treatment would become significant only at late stages.[14] On the other hand, this long-lasting presence of photoreceptors generates potentially a long therapeutic window. More importantly, the early alterations to the photoreceptor morphology, that is, the absence of the outer retinal bands on OCT scans early in the disease process, represent a useful readout parameter to study treatment outcome at an early age.[27]

ONL thinning has already been shown for other *Rpgr* mouse models, for example, in the rd9 mutant mice becoming clear and significant around 12 months

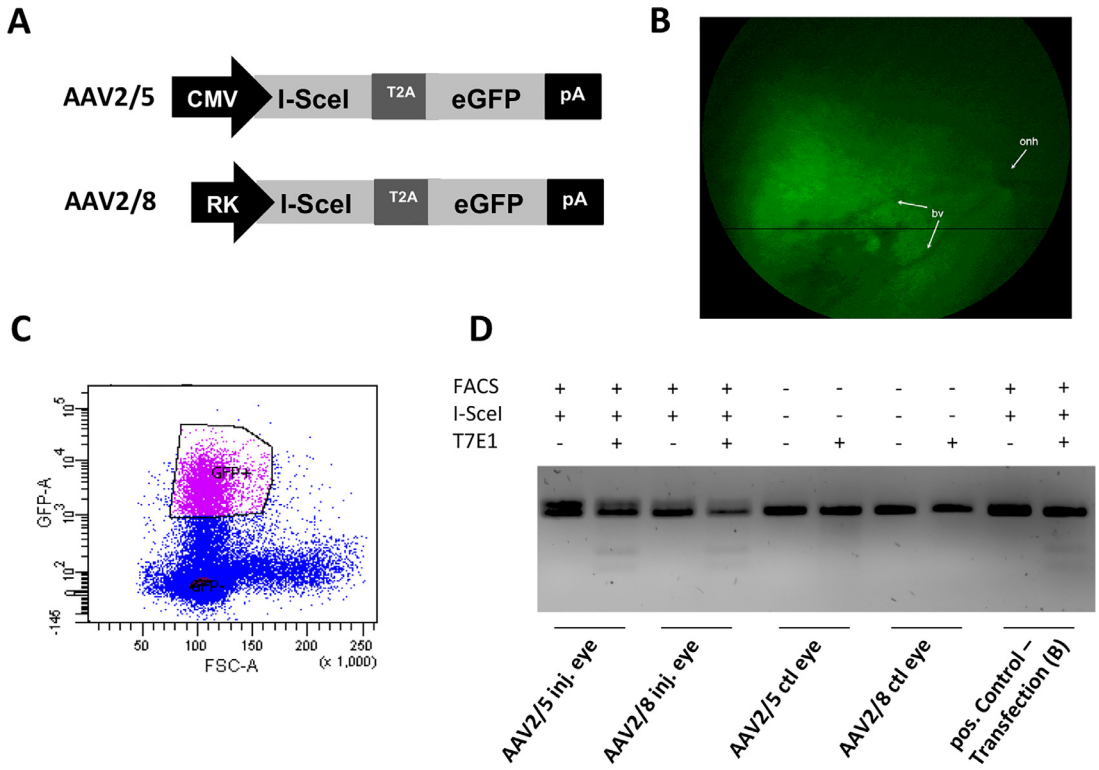

Fig 8. Genome editing at the I-SceI site in vivo. (**A**) The two AAV vector constructs are depicted. The AAV2/5 vector contained an expression cassette in which I-SceI and GFP, linked by a T2A linker, were under the control of a CMV promoter, thus allowing transgene expression in all transduced cells. The AAV2/8 vector contained an expression cassette in which I-SceI and GFP were under the control of a Rhodopsin kinase (RK) promoter, which ensures photoreceptor specific transgene expression. (**B**) In vivo fluorescence image from transduced retina showing the GFP expression in the injected area. onh: optic nerve head; bv: blood vessel. (**C**) FACS data showing the enrichment of the GFP positive cell population. (**D**) DNA repair events following AAV mediated I-SceI gene transfer and subsequent enrichment of the GFP positive cells resulted in measurable NHEJ activity in both injected eyes, while control eyes did not reveal such activity. Positive control experiment was the in vitro experiment described in Fig 7. "+" and "−" refers to whether FACS enrichment, I-sceI expression and T7 endonuclease digestion took place or not. DNA, deoxyribonucleic acid; FACS, fluorescent activated cell sorting; NHEJ, nonhomologous end-joining.

of age.[25] The *Rpgr* knock-out mouse model developed by Hong et al[23] also showed a thinning of the photoreceptor nuclear layer with a loss of 2 rows of nuclei on average by the age of 6 months, an observation that was also reported by other groups.[28,29] These findings suggest that frame shift mutations in the *Orf15* (like the ones occurring in the rd9 model and the model presented here) lead to milder forms of degeneration compared to knock-out mutations, which may be related to a residual function of the altered protein.

Concerning the function of the photoreceptors, ERG amplitudes in our model are reduced in scotopic a-wave as well as b-wave, starting at the age of 12 months, coinciding with the start of photoreceptor nuclear cell loss. Photopic flicker responses are similarly reduced in older animals. These observations indicate that both types of photoreceptors, rods and cones are involved in the pathology. The impact of aging on function is relatively small, since age-matched wild type animals only show a slight reduction of the measured amplitudes. Similarly, functional analysis showed reduced amplitudes for all known *Rpgr* mouse models at later stages of the disease.[25,23,28,30,31] Similar to our model, the rd9 model shows a moderate but constant reduction of a-wave as well as b-wave amplitudes until the age of 24 months.[25] The knock-out mouse model by Hong et al shows reduced a-wave amplitudes for rods as well as for cones at the age of 6 months,[23] while the model established by Brunner et al shows only a mild reduction of the scotopic a-wave from the age of 3 months onwards and no alteration of the scotopic b-wave.[28]

The pathologies observed in our model or in the published *rd9* mouse are less severe than those observed in human patients. One base pair frame shifts with long C-terminal protein chain alteration seem to be reason

for the most severe phenotypes in humans, but only a mild phenotype in mice (this study).[25] Recent in vivo analysis of human retinae with SD OCT technology revealed early ONL thinning outside the fovea despite the presence of identifiable ISe (inner segment retinoid) and OS structures,[5] which was also observed in other studies.[32,33] In contrast, the murine ISe and OS structures, which can be distinguished in wild type mice, are not visible in mutant retinae. This has also been observed in the knock-out mouse generated by Huang et al.[29] Since current understanding of functional correlates identifies ISe as a valid morphologic indicator of functional photoreceptors in OCT scans of humans, this is not the case for murine OCT scans. In young affected animals of our model, ERG recordings are unchanged, yet the ISe band is not detectable from the beginning.

In summary, the newly generated mouse model displays a degenerative phenotype with thinning of retinal layers starting at 9 months and loss of photoreceptor function beginning at 12 months of age, indicating the activation of a similar or at least closely related pathologic pathway like in human patients. Therefore, this model is an eligible model for the development of gene-therapeutic applications in the future. In addition, it may help to gain further insight into the pathological mechanisms involved in retinal degeneration and the expression pattern of mutant Rpgr-Orf15. Moreover, the influence of point mutations in the *ORF15* repetitive region on expression and splicing of the mRNA, as well as the biochemical reason for the toxicity of emerging proteins could be addressed by the model in further experiments. Finally, the use of this model to study genome editing in the degenerating retina in vivo using all nuclease classes currently available renders the model very important.

ACKNOWLEDGMENTS

The authors thank Susanne Kreutzer (MPI Bad Nauheim) for ES cell injection, Dr. Christoph Friedburg (JLU Giessen) for technical support with the ERG. The authors thank Prof. Hackstein, Dr. Baal, and Gaby Michel, FACS core facility, JLU Giessen, for help to perform the FACS analysis. This study was supported by research grants from the University Medical Centre Giessen and Marburg (UKGM, 13/2011GI), and the Else-Kröner-Fresenius Foundation (2013_A270). The study was also in part supported by the ERC starting grant STG 2012-311244 to KS. HK was supported by grant from the National Institutes of Health NEI RO1-EY022372.

All authors have read the journals policy on disclosure of potential conflict of interest. There is nothing to declare. All authors have read the journal's authorship agreement.

SUPPLEMENTARY MATERIALS

Supplementary data associated with this article can be found in the online version at https://doi.org/10.1016/j.trsl.2018.08.006.

REFERENCES

1. Hartong DT, Berson EL, Dryja TP. Retinitis pigmentosa. Lancet 2006;368:1795–809. https://doi.org/10.1016/S0140-6736(06)69740-7 London, England.
2. Sharon D, Sandberg Ma, Rabe VW, Stillberger M, Dryja TP, Berson EL. RP2 and RPGR mutations and clinical correlations in patients with X-linked retinitis pigmentosa. Am J Hum Genet 2003;73:1131–46. https://doi.org/10.1086/379379.
3. Shu X, Black GC, Rice JM, Hart-holden N, Jones A, Grady AO, et al. Mutation update rpgr mutation analysis and disease: an update. 2007;28: 322−28. doi:10.1002/humu
4. Lorenz B, Andrassi M, Kretschmann U. Phenotype in two families with RP3 associated with RPGR mutations. Ophthalmic Genet 2003;24:89–101. https://doi.org/10.1076/opge.24.2.89.14001.
5. Birch DG, Locke KG, Wen Y, Locke KI, Hoffman DR, Hood DC. Spectral-domain optical coherence tomography measures of outer segment layer progression in patients with x-linked retinitis pigmentosa. JAMA Ophthalmol 2013;131:1143–50. https://doi.org/10.1001/jamaophthalmol.2013.4160.
6. Vervoort R, Lennon a, Bird aC, Tulloch B, Axton R, Miano MG, et al. Mutational hot spot within a new RPGR exon in X-linked retinitis pigmentosa. Nat Genet 2000;25:462–6. https://doi.org/10.1038/78182.
7. Adams NA, Awadein A, Toma HS. The retinal ciliopathies. Ophthalmic Genet 2007;28:113–25. https://doi.org/10.1080/13816810701537424.
8. Khanna H, Hurd TW, Lillo C, Shu X, Parapuram SK, He S, et al. RPGR-ORF15, which is mutated in retinitis pigmentosa, associates with SMC1, SMC3, and microtubule transport proteins. J Biol Chem 2005;280:33580–7. https://doi.org/10.1074/jbc.M505827200.
9. Rao KN, Li L, Anand M, Khanna H. Ablation of retinal ciliopathy protein RPGR results in altered photoreceptor ciliary composition. Sci Rep 2015;5:11137. https://doi.org/10.1038/srep11137 Nature Publishing Group.
10. Rao KN, Zhang W, Li L, Anand M, Khanna H. Prenylated retinal ciliopathy protein RPGR interacts with PDE6delta and regulates ciliary localization of Joubert syndrome-associated protein INPP5E. Hum Mol Genet 2016;25:4533–45. https://doi.org/10.1093/hmg/ddw281 England.
11. Zhang Q, Acland GM, Wu WX, Johnson JL, Pearce-Kelling S, Tulloch B, et al. Different RPGR exon ORF15 mutations in Canids provide insights into photoreceptor cell degeneration. Hum Mol Genet 2002;11:993–1003, Available http://www.ncbi.nlm.nih.gov/pubmed/11978759.
12. Rao KN, Anand M, Khanna H. The carboxyl terminal mutational hotspot of the ciliary disease protein RPGRORF15 (retinitis pigmentosa GTPase regulator) is glutamylated in vivo. Biol Open 2016;15:1–5. https://doi.org/10.1242/bio.016816.
13. Sun X, Park JH, Gumerson J, Wu Z, Swaroop A, Qian H, et al. Loss of RPGR glutamylation underlies the pathogenic mechanism of retinal dystrophy caused by *TTLL5* mutations. Proc Natl Acad Sci 2016;113:E2925–34. https://doi.org/10.1073/pnas.1523201113.
14. Wu Z, Hiriyanna S, Qian H, Mookherjee S, Campos MM, Gao C, et al. A long-term efficacy study of gene replacement therapy for RPGR-associated retinal degeneration. Hum Mol Genet 2015;24:3956–70. https://doi.org/10.1093/hmg/ddv134.

15. Beltran WA, Cideciyan AV, Boye SE, Ye G-J, Iwabe S, Dufour VL, et al. Optimization of retinal gene therapy for X-linked retinitis pigmentosa due to RPGR mutations. Mol Ther 2017;25:1866–80. https://doi.org/10.1016/j.ymthe.2017.05.004.
16. Fischer MD, McClements ME, Martinez-Fernandez dela, Camara C, Bellingrath J-S, Dauletbekov D, et al. Codon-optimized RPGR improves stability and efficacy of AAV8 gene therapy in two mouse models of X-linked retinitis pigmentosa. Mol Ther 2017;25:1854–65. https://doi.org/10.1016/j.ymthe.2017.05.005.
17. Maeder ML, Gersbach CA. Genome-editing technologies for gene and cell therapy. Mol Ther Off J Am Soc Gene Cell Ther 2016;24:430–46. https://doi.org/10.1038/mt.2016.10.
18. Yanik M, Müller B, Song F, Gall J, Wagner F, Wende W, et al. In vivo genome editing as a potential treatment strategy for inherited retinal dystrophies. Prog Retin Eye Res 2017;56. https://doi.org/10.1016/j.preteyeres.2016.09.001.
19. Mefferd AL, Kornepati AVR, Bogerd HP, Kennedy EM, Cullen BR. Expression of CRISPR/Cas single guide RNAs using small tRNA promoters. RNA 2015;21:1683–9. https://doi.org/10.1261/rna.051631.115.
20. Bartsevich V, Jantz D, Smith J, Nicholson M. Treatment of Retinitis Pigmentosa Using Engineered Meganucleases. WO/2017/044649, 2017.
21. Samardzija M, von Lintig J, Tanimoto N, Oberhauser V, Thiersch M, Remé CE, et al. R91W mutation in Rpe65 leads to milder early-onset retinal dystrophy due to the generation of low levels of 11-cis-retinal. Hum Mol Genet 2008;17:281–92. https://doi.org/10.1093/hmg/ddm304.
22. Liu P, Jenkins Na, Copeland NG. A highly efficient recombineering-based method for generating conditional knockout mutations. Genome Res 2003;13:476–84. https://doi.org/10.1101/gr.749203.
23. Hong DH, Pawlyk BS, Shang J, Sandberg Ma, Berson EL, Li T. A retinitis pigmentosa GTPase regulator (RPGR)-deficient mouse model for X-linked retinitis pigmentosa (RP3). Proc Natl Acad Sci USA 2000;97:3649–54. https://doi.org/10.1073/pnas.060037497.
24. Seeliger MW, Grimm C, Ståhlberg F, Friedburg C, Jaissle G, Zrenner E, et al. New views on RPE65 deficiency: the rod system is the source of vision in a mouse model of Leber congenital amaurosis. Nat Genet 2001;29:70–4. https://doi.org/10.1038/ng712.
25. Thompson Da, Khan NW, Othman MI, Chang B, Jia L, Grahek G, et al. Rd9 is a naturally occurring mouse model of a common form of retinitis pigmentosa caused by mutations in RPGR-ORF15Vavvas D, editor PLoS One 2012;7:e35865. https://doi.org/10.1371/journal.pone.0035865.
26. Wright RN, Hong D-H, Perkins B. Misexpression of the constitutive Rpgr(ex1-19) variant leads to severe photoreceptor degeneration. Investig Ophthalmol Vis Sci 2011;52:5189–201. https://doi.org/10.1167/iovs.11-7470.
27. Beltran Wa, Cideciyan aV, Lewin aS, Iwabe S, Khanna H, Sumaroka a, et al. Gene therapy rescues photoreceptor blindness in dogs and paves the way for treating human X-linked retinitis pigmentosa. Proc Natl Acad Sci 2012;109:2132–7. https://doi.org/10.1073/pnas.1118847109.
28. Brunner S, Skosyrski S, Kirschner-Schwabe R, Knobeloch K-P, Neidhardt J, Feil S, et al. Cone versus rod disease in a mutant Rpgr mouse caused by different genetic backgrounds. Investig Ophthalmol Vis Sci 2010;51:1106–15. https://doi.org/10.1167/iovs.08-2742.
29. Huang WC, Wright AF, Roman AJ, Cideciyan AV, Manson FD, Gewaily DY, et al. RPGR-associated retinal degeneration in human X-linked RP and a murine model. Investig Ophthalmol Vis Sci 2012;53:5594–608. https://doi.org/10.1167/iovs.12-10070.
30. Brunner S, Colman D, Travis AJ, Luhmann UFO, Shi W, Feil S, et al. Overexpression of RPGR leads to male infertility in mice due to defects in flagellar assembly. Biol Reprod 2008;79:608–17. https://doi.org/10.1095/biolreprod.107.067454.
31. Hong D-H. Dominant, gain-of-function mutant produced by truncation of RPGR. Investig Ophthalmol Vis Sci 2004;45:36–41. https://doi.org/10.1167/iovs.03-0787.
32. Aleman TS, Cideciyan AV, Sumaroka A, Schwartz SB, Roman AJ, Windsor EaM, et al. Inner retinal abnormalities in X-linked retinitis pigmentosa with RPGR mutations. Investig Ophthalmol Vis Sci 2007;48:4759–65. https://doi.org/10.1167/iovs.07-0453.
33. Lorenz B, Preising M, Stieger K. Retinal blinding disorders and gene therapy−molecular and clinical aspects. Curr Gene Ther 2010;10:350–70, Available http://www.ncbi.nlm.nih.gov/pubmed/20712581.